DESIGN AND OPTIMIZATION OF THE MEDAUSTRON SYNCHROTRON MAIN DIPOLES

B. Langenbeck, C. Siedler, M. Stockner, EBG-MedAustron, Wiener Neustadt, Austria
T. Zickler , CERN, Geneva, Switzerland.

Abstract

MedAustron, a future centre for ion-therapy and research in Austria will comprise an accelerator facility based on a synchrotron for the delivery of protons and light ions for cancer treatment and for clinical and non-clinical research [1]. The main dipole for the synchrotron went through an extensive design process to meet the stringent requirements. The local and integrated field quality was optimized. The residual field levels in the magnet gap were calculated and the dynamic behaviour of the dipole magnet was studied, both in 2D and 3D, using OPERA. The pole profile has been optimized to reduce sextupolar components in the integrated field by adjusting the shims on the pole edge. A Rogowski-profile at the pole ends and the use of stainless-steel tension straps shall enhance the dynamic behaviour and guarantee a small time constants. Appropriate pole-end shimming will be used to compensate for residual multi-pole components and to fine-tune the magnetic length. The results of this comprehensive design study are summarized in this paper.

REQUIREMENTS

The heart of the MedAustron accelerator is a synchrotron operating at a repetition rate of 1 Hz. The synchrotron will have 16 main dipole magnets and 24 quadrupole magnets. The required field levels for the dipoles reach from 90 mT to 1.5 T. Field quality at all field levels shall be better than $\pm 2 \cdot 10^{-4}$ in a good field region of ± 60 mm horizontally and ± 30 mm vertically. The 16 dipoles will be powered in series and shall have therefor a uniform magnetic length within $1 \cdot 10^{-3}$. To ensure the 1Hz operation, the field stabilization time after ramping with 3 T/s shall be below 100 ms [2].

DESIGN CONSIDERATIONS

With respect to pulsed operation, the yoke of the magnet shall be laminated. Special attention was given to the material used for the magnet lamination. Low-carbon electrical steel has been selected with a suitable amount of 0.5 % silicon to increase its electrical resistivity. The requirements on the thickness tolerances are high (maximal variation of 7 μm perpendicular to the rolling direction) to increase and unify the packing factor of the yokes to 98% ±0.1%.

During the design work three cases have been studied: a Bedstead coil with oblong cross-section, a race-track coil with oblong cross-section and a race-track coil with quadratic cross-section. Finally the quadratic race-track coil was chosen as bending homogeneity and magnet length benefit from this design.

To cope with the stringent requirements of a medical machine special attention was given to the integrated field quality and dynamic effects.

The integrated field quality was improved by iterating 2D and 3D simulations to optimize the lamination cross section. Dynamic effects were studied first in 2D and later in 3D. All field calculations were performed with the software OPERA from VectorFields/Cobham, Kidlington Oxford, England.

LAYOUT OF MANGET LAMELLA

The pole profile was designed such that all field lines within the pole are approximately parallel. This avoids magnetic saturation of the pole periphery at high field levels almost completely. At the edge of the pole shims are introduced which are continued by a Rogowski profile [3]. The layout of the final lamella with flux lines is shown in Fig. 1.
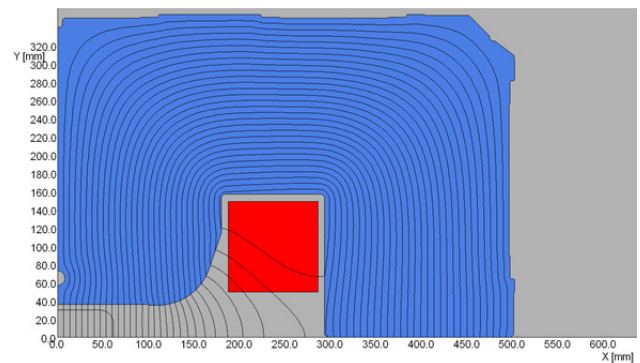

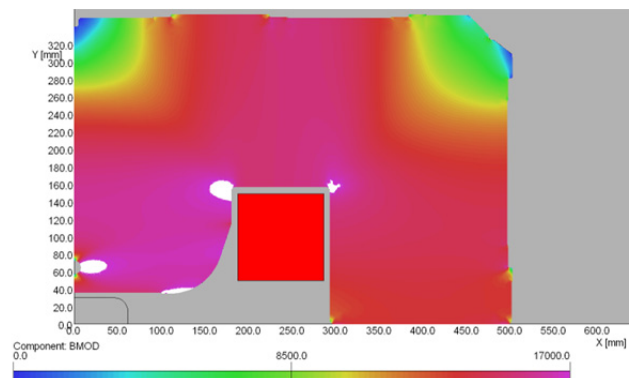Figure 1: Plan view of half-lamella with flux lines.

Figure 2: Flux density distribution in lamella at 1.5 T.

Fig. 2 shows the flux density distribution in the pole and the yoke at B = 1.5 T. At this field level, the shim region starts to saturate. To minimize a corresponding deterioration of the field quality, an additional central

saturation zone was intentionally introduced by a hole above the pole centre.

The optimization of the field quality was performed using BH-curves representing the anisotropic behaviour of the steel permeability. Fig. 3 shows the field quality along the good field region. Permeability values measured in steel rolling direction were used in vertical magnet direction. In horizontal direction values measured perpendicular to rolling direction were used. The 1 mm thick steel sheets are of type Isovac 1300-100A supplied by Voest-Alpine, Austria. This material has an unusual small variation of permeability and coercivity. The permeability variation is about 4% and the coercivity variation is ±2 A/m.
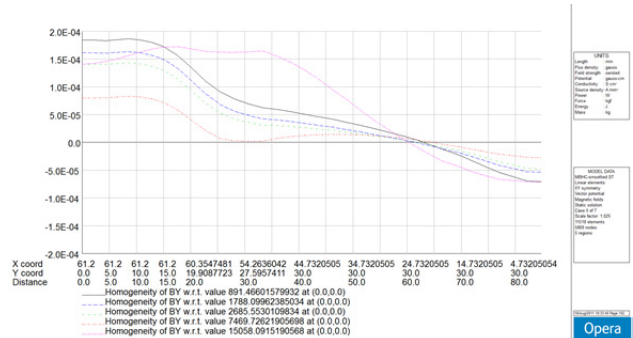

Figure 3: Field homogeneity along the good field region.

The curves in Fig. 3 represent the field homogeneity at four different field levels that are asymmetric with respect to the zero level. The reason is that at low fields the field lines tend to concentrate to find high permeability values. At high field levels the asymmetry was introduced to compensate for multi-pole errors in the integrated field.

PARTICLE DEFLECTION ERROR

To determine the radial bending characteristics of the dipole, a model giving the full geometry including the curvature of the yoke was used. Particles were started in the magnet centre perpendicularly to the vertical mid plane. The energy has been adjusted to get a deflection angle of 11.25° for the central particle.

Compared to the first design that only fulfilled the 2D field homogeneity requirements the relative deflection error could be reduced by a factor of 5 in the final design. This was possible due to the increase of the field level at the horizontal outer limit of the good field region by modifying the parameters of pole shims and central hole (see Fig. 3).

The result of the optimized model is shown in Fig. 4. The graphs are asymmetric with respect to $x = 0$ indicating a quadrupole component due to the stray field distribution at the magnet ends: the integrated field seen by particles starting at $x < 0$ is smaller than for particles starting at $x > 0$.
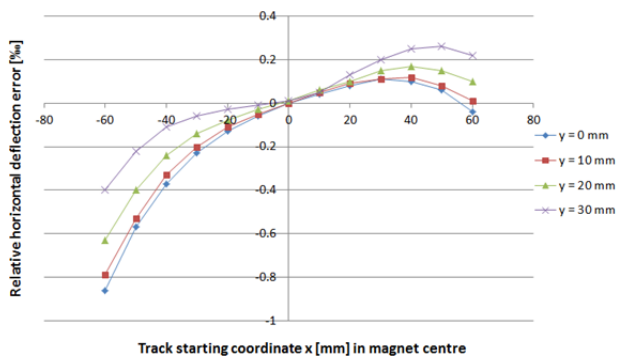

Figure 4: Relative deflection error at 1.5 Tesla.

The remaining deflection errors will be systematically compensated by pole end shimming during magnetic measurements in order to reach the required field quality of $\pm 2 \cdot 10^{-4}$.

TIME DEPENDENT SIMULATIONS

2D Time Dependent Simulation

Special attention was given to eddy currents in the yoke during ramping the magnetic field. Simulations of the magnet have shown that eddy currents in the tension straps which are made of ferro-magnetic material and welded along the yoke can cause an attenuation of the field in the gap at and after ramp end in the range of several per mill. This results in a field stabilization time in the order of seconds. Therefore, the straps must be made of non-magnetic stainless steel to avoid attracting flux.

The mechanism behind this effect can be explained by eddy currents in the non-laminated, ferro-magnetic tension straps while ramping the magnetic field, which are preventing the magnetic flux to penetrate these regions (Fig. 5). Hundred seconds after the ramp end (Fig. 6) the eddy currents have decayed and the magnetic flux can use the tension straps as additional path. This reduces the reluctance of the magnetic circuit resulting in a field increase in the gap.
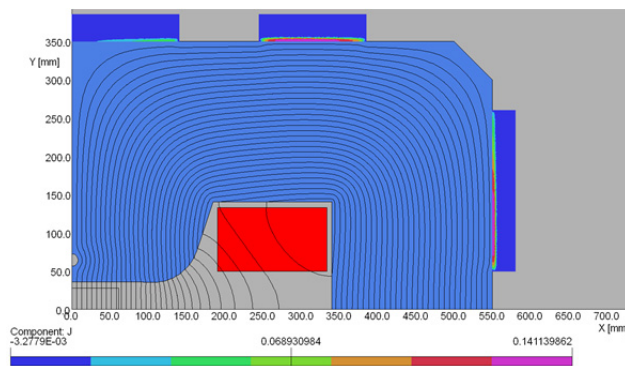

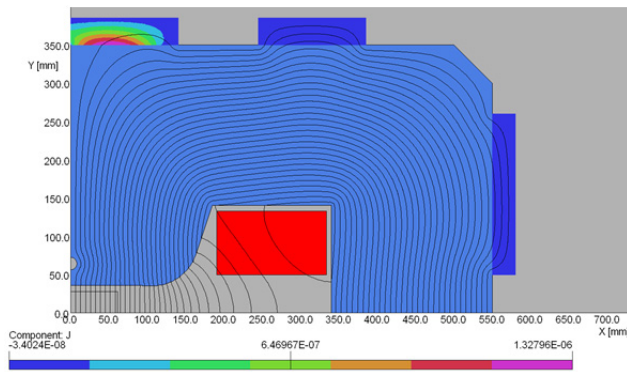Figure 5: Flux lines and eddy current distribution in the tension straps at ramp end.

Figure 6: Flux lines and eddy currents in tension straps hundred seconds after ramp end.

3D Time Dependent Simulation

The stray fields around the extremities of the magnet approach the poles with field components perpendicular to the lamination surfaces. This introduces eddy currents in the laminations and a retardation of the field integral during the ramp. The field at the end of the ramp is attenuated by several per-mills before it reaches its final stable value after several seconds. A Rogowski profile in longitudinal direction at the pole ends forces the flux lines parallel to the lamination direction resulting in a minimization of this field retardation.

To reduce the mesh size and the solver run time a straight model of the magnet has been prepared for the simulations and a field ramp of 500 ms from zero to 1.5 T was programmed with OPERA's transient solver ELEKTRA. With the help of Vectorfield's support team, major effort was put into the refinement of the mesh, especially for the appropriate layering of the Rogowski profiles. The axial conductivity was set to 1 ppm of the Isovac 1300-100A conductivity of 3636 S/mm. The calculation time could be reduced to 80 hours on a 2.3 GHz, 8 GB RAM office PC.
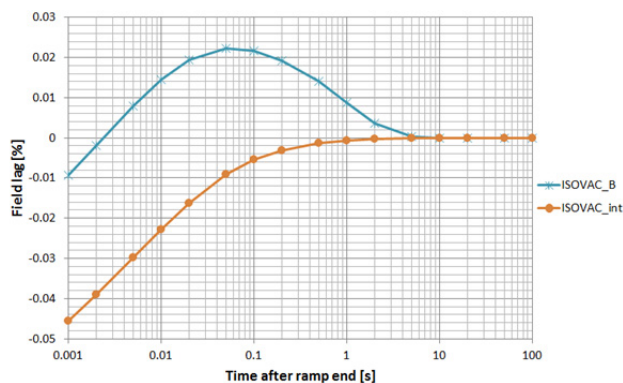

Figure 7: Local field and integrated field development after ramping the field to 1.5 T in 500 ms.

Fig. 7 shows the development of the local field in the magnet centre and the integrated field after ramp end. The field integral (Isovac_int) approaches the 1.5 T level to $1 \cdot 10^{-4}$ within 50 ms after ramp end. The temporary overshoot of the local field in the magnet centre results from the assumed low axial conductivity representing the

laminated yoke structure. Hence, the eddy current flow is mainly restricted to the XY-plane. Fig. 8 shows schematically the induced eddy currents (upper blue). As the return currents (lower blue) are closer to the magnet gap they act to increase the magnetic flux density in the magnet centre until the eddy currents have decayed.
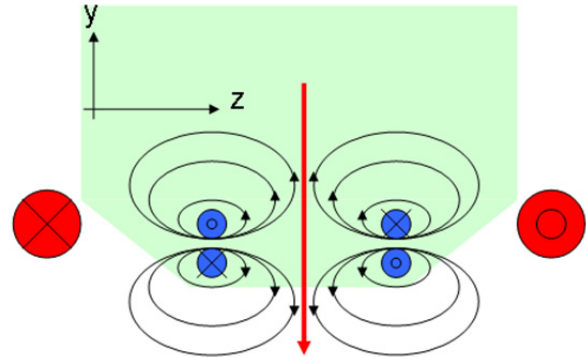

Figure 8: Field contributions from the primary coil and eddy currents in the YZ-plane.

SUMMARY

Simulation results show that the specified requirements concerning the local field quality and field stabilization time can be fulfilled. The remaining deflection error in the integrated field will be corrected on the pre-series magnet.

In addition, studies on the electrical steel properties, the packing factor tolerances and the residual field have been performed. Tight tolerances on the steel quality and a shuffling procedure for the laminations have been defined to further enhance the performance of these magnets.

OUTLOOK

The delivery of the two pre-series magnets is foreseen by the end of the year 2011. During the magnetic measurements, the integrated field quality and magnetic length will be adjusted by adaptive pole end shimming. The final end shim profile which will be determined on the pre-series magnets will then be systematically applied to all series magnets, so that only an adjustment of the magnetic length has to be performed.

The commissioning of the synchrotron is planned for 2013.

REFERENCES

[1] M. Benedikt, A. Wrulich, "MedAustron-Project overview and status", Eur. Phys. J. Plus, 2011, 126:69

[2] P. J. Bryant, L. Badano, M. Benedikt, M. Crescenti, P. Holy, A.T. Maier, M. Pullia, S. Reimoser, S. Rossi, G. Borri, P. Knaus, F. Gramatica, M. Pavlovic and L. Weisser, "Proton-Ion Medical Machine Study (PIMMS), 2", CERN-PS-2000-007-DR, Aug. 2000, p. 340.

[3] H. A. Enge, "Converting an ion-optical layout into the design of a practical magnet system", Proc. Int. Symp. Magn. Techn, Stanford 1965, p. 84.